THE JOURNAL OF BIOLOGICAL CHEMISTRY VOL. 287, NO. 24, pp. 20534–20544, June 8, 2012

Mitochondrial Dysfunction in Skeletal Muscle of Amyloid Precursor Protein-overexpressing Mice*

Received for publication, March 9, 2012, and in revised form, April 6, 2012 Published, JBC Papers in Press, April 19, 2012, DOI 10.1074/jbc.M112.359588

Simona Boncompagni[‡1], Charbel E.-H. Moussa[§1], Ezra Levy[¶], Matthew J. Pezone[¶], José R. Lopez[‖], Feliciano Protasi[‡], and Alexander Shtifman[¶2]

From the [‡]CeSI-Centro Scienze dell'Invecchiamento and DNI-Department of Neuroscience and Imaging, University Gabriele d'Annunzio, I-66100 Chieti, Italy, the [§]Department of Neuroscience, Department of Biochemistry and Molecular & Cell Biology, Georgetown University School of Medicine, Washington, D.C. 20057, the [‖]Department of Anesthesia. Brigham & Women's Hospital, Boston, Massachusetts 02115, and the [¶]Department of Neurology, Steward St. Elizabeth's Medical Center, Tufts University School of Medicine, Boston, Massachusetts 02135

Background: Intracellular accumulation of β-amyloid is a key step in pathogenesis of the inclusion body myositis (IBM).
Results: Intramyofiber accumulation of β-amyloid in MCK-βAPP mice leads to structural and functional mitochondrial abnormalities.
Conclusion: Mitochondrial abnormalities precede IBM-related histological and motor deficits in MCK-βAPP mice.
Significance: The diminished mitochondrial function may play a key role during the β-amyloid mediated pathogenesis in IBM.

Inclusion body myositis, the most common muscle disorder in the elderly, is partly characterized by abnormal expression of amyloid precursor protein (APP) and intracellular accumulation of its proteolytic fragments collectively known as β-amyloid. The present study examined the effects of β-amyloid accumulation on mitochondrial structure and function of skeletal muscle from transgenic mice (MCK-βAPP) engineered to accumulate intramyofiber β-amyloid. Electron microscopic analysis revealed that a large fraction of myofibers from 2–3-month-old MCK-βAPP mice contained numerous, heterogeneous alterations in mitochondria, and other cellular organelles. [^{1}H-decoupled]^{13}C NMR spectroscopy showed a substantial reduction in TCA cycle activity and indicated a switch from aerobic to anaerobic glucose metabolism in the MCK-βAPP muscle. Isolated muscle fibers from the MCK-βAPP mice also exhibited a reduction in cytoplasmic pH, an increased rate of ROS production, and a partially depolarized plasmalemma. Treatment of MCK-βAPP muscle cells with Ru360, a mitochondrial Ca^{2+} uniporter antagonist, reversed alterations in the plasmalemmal membrane potential (V_m) and pH. Consistent with altered redox state of the cells, treatment of MCK-βAPP muscle cells with glutathione reversed the effects of β-amyloid accumulation on Ca^{2+} transient amplitudes. We conclude that structural and functional alterations in mitochondria precede the reported appearance of histopathological and clinical features in the MCK-βAPP mice and may represent key early events in the pathogenesis of inclusion body myositis.

Inclusion body myositis (IBM)[3] is the most common muscle disease in the aging population (1). A cardinal feature of IBM is the presence of endomysial inflammation characterized by the invasion of myofibers by $CD8^+$ cytotoxic T cells. In addition to the immunopathogenic events, there is an equally strong degenerative process in IBM muscle evidenced by the presence of sparsely occurring vacuoles, atrophic muscle fibers, and loss of muscle mass. Although the pathogenesis of IBM is still unknown, it appears that skeletal muscle tissue accumulates numerous misfolded proteins that are also associated with Alzheimer disease (2–5). Among these proteins, an abnormal expression of the amyloid precursor protein (APP) and the intracellular accumulation of its proteolytic products, collectively known as β-amyloid (Aβ), may represent key events in the pathogenic process of IBM (6–8). Ultrastructurally, β-amyloid deposits are localized in vacuolated muscle fibers often associated with multiprotein inclusions (2, 9). In addition to vacuoles and inclusions, mitochondrial abnormalities and decreased cytochrome *c* oxidase activity have been shown to be mediated by Aβ accumulation in cultured muscle fibers driven to overexpress APP (10, 11). Although the role of impaired mitochondrial function in pathophysiology of IBM has not been fully defined, there are indications of mitochondrial participation in the development of muscle disease (12, 13).

The consequences of intracellular Aβ accumulation in skeletal muscle can be now studied with transgenic mice (MCK-βAPP) that are engineered to selectively overexpress holo-APP, thus accumulating a substantial amount of APP proteolytic fragments including C99, $A\beta_{1-40}$, and $A\beta_{1-42}$ in the muscle tissue (14–16). The MCK-βAPP transgenic mice present age-dependent myopathic features of IBM, including angulated

* This work was supported, in whole or in part, by National Institutes of Health Grants K01-AR053114 and R03-AR054519 (to A. S.) and AG30378 (to C. M.). This work was also supported by Research Grant GGP08153 from the Italian Telethon ONLUS Foundation (to F. P.).
[1] These authors contributed equally to this work.
[2] To whom correspondence should be addressed: Dept. of Neurology, Steward St. Elizabeth's Medical Center, Tufts University School of Medicine, 736 Cambridge St., CBR-406, Boston, MA 02135. Tel.: 617-789-2678; Fax: 617-789-3111; E-mail: alex.shtifman@steward.org.

[3] The abbreviations used are: IBM, inclusion body myositis; APP, amyloid precursor protein; Aβ, β-amyloid; EDL, extensor digitorum longus; FDB, flexor digitorum brevis; DCF, 2′,7′-dichlorofluorescein; RyR, ryanodine receptor Ca^{2+} release channel; SR, sarcoplasmic reticulum; SERCA, sarcoplasmic/endoplasmic reticulum Ca^{2+}-ATPasel; ROS, reactive oxygen species; TMRE, tetramethylrhodamine, ethyl ester; DHPR, dihydropyridine receptor.

fibers, inflammation, and deficits in motor performance (15, 16). In addition to gross structural and functional abnormalities, it has now been established that age-dependent dysregulation of cytoplasmic Ca^{2+} homeostasis and alterations in the function of the excitation-contraction coupling process represent presymptomatic events in Aβ-affected skeletal muscle (17). Although the downstream effects of Ca^{2+} dysregulation mediated by Aβ are still under investigation, potential targets could include processes that are modulated by Ca^{2+} inside the mitochondria. It is well documented that disruption of cytoplasmic Ca^{2+} handling can have unfavorable effects on mitochondrial function (18). Under normal physiological conditions, an increase in Ca^{2+} transport from the cytoplasm into the mitochondrial matrix exerts a positive effect on mitochondrial function (19, 20), whereas excessive Ca^{2+} uptake by mitochondria can lead to an overload of Ca^{2+} within the mitochondrial matrix. Long term mitochondrial Ca^{2+} overload can ultimately lead to swelling of the matrix, rupture of the outer mitochondrial membrane, and a loss of mitochondrial membrane potential ($\Delta\Psi_{mito}$) (21, 22). Combined effects of mitochondrial Ca^{2+} overload and direct, deleterious effects that Aβ exerts on mitochondria (23–28) could have detrimental implications on cellular energy production as well as overall cellular function (18).

In the current study, we investigated the effects of intracellular Aβ accumulation on skeletal muscle mitochondria from 2–3-month-old MCK-βAPP mice. A young age group was specifically chosen because, based on previous investigations, young MCK-βAPP mice do not manifest IBM-like features such as inflammation and motor deficits (15, 16) but already exhibit alterations in Ca^{2+} homeostasis and excitation-contraction coupling (17). Using the MCK-βAPP mouse model, we demonstrate that structural and functional alterations in mitochondria precede the reported appearance of histopathological and clinical features in the MCK-βAPP mice and may represent key early events in the pathogenesis of IBM.

EXPERIMENTAL PROCEDURES

Mice—Age-matched, hemizygous MCK-βAPP (15) and WT (control) mice were used in this study following a protocol approved by the St. Elizabeth's Medical Center Institutional Animal Care and Use Committee. All of the mice were generated by breeding a WT female with a heterozygous MCK-βAPP transgenic male, thus producing litters containing WT and MCK-βAPP mice with an isogenic background. The mice were euthanized by pentobarbital-based euthanasia solution overdose delivered by intraperitoneal injection followed by a cervical dislocation.

Fixation and Embedding for Electron Microscopy—The skin was removed from both legs, and intact extensor digitorum longus (EDL) muscles were dissected, pinned through the tendons in a Sylgard-coated (Dow Corning) dish at resting length and fixed with 3.5% glutaraldehyde in 0.1 M sodium cacodylate buffer, pH 7.2, at room temperature. Specimens were then stored in fixative at 4 °C. Small bundles of fixed muscle fibers were post-fixed in 2% OsO_4 in the same sodium cacodylate buffer for 1–2 h at 4 °C and block-stained in saturated uranyl acetate. After dehydration, the specimens were embedded in an epoxy resin (Epon 812). Ultrathin sections (~50 nm) were cut in an ultramicrotome Leica Ultracut R (Leica Microsystem, Vienna, Austria) using a Diatome diamond knife (Diatome Ltd., CH-2501, Biel, Switzerland). Later, sections were stained in 4% uranyl acetate and lead citrate solutions. All of the sections were examined with a FP 505 Morgagni Series 268D electron microscope (Philips, Brno, Czech Republic) at 60 kV equipped with a Megaview III digital camera and Soft Imaging System (Munster, Germany).

Aβ ELISA—Human specific $Aβ_{1-40}$ and $Aβ_{1-42}$ ELISA (BIOSOURCE) was performed using 50 μl (1 μg/μl) of whole muscle lysates detected with 50 μl of human $Aβ_{1-40}$ or $Aβ_{1-42}$ primary antibody (3 h) and 100 μl of anti-rabbit antibody (30 min) at room temperature. The extracts were incubated with stabilized Chromogen for 30 min at room temperature, and the solution was stopped and read at 450 nm (Multiskan FC; Thermo Fisher) according to the manufacturer's protocol.

High Frequency ^{13}C NMR Spectroscopy—The animals were fasted overnight with free access to tap water and were intraperitoneally injected with [1-^{13}C]pyruvate solution (0.5 mol/L) over 10 s (0.3 ml/25–30 g of body weight; 200 mg/kg). 45 min later, the animals were sacrificed, and the hamstring muscles were excised and immediately frozen in N_2. Muscle tissue was homogenized in 5% ice-cold perchloric acid (50 mM NaH_2PO_4). After homogenization and lyophilization, the extracts were resuspended in 0.65 ml of D_2O containing 2 mM sodium [^{13}C]formate as internal intensity and chemical shift reference (δ 171.8). Metabolite pool size was identified on ^1H[^{13}C-decoupled] NMR spectra. Peak areas were adjusted for nuclear Overhauser effect, saturation, and natural abundance effects and quantified by reference to [^{13}C]formate. Metabolite pool sizes were determined by integration of resonances in fully relaxed 400 MHz [^{13}C-decoupled]^1H spectra using *N*-acetylaspartate as internal intensity reference. Incorporation of ^{13}C into isotopomers was measured in reference to [^{13}C]formate. All of the data were collected on a 9.7-Tesla Varian Spectrometer with dual $^{13}C/^1H$ probe. [^{13}C-decoupled]^1H spectra was acquired with 3000 scans: pulse width, 45°; relaxation delay, 1 s; line broadening, 0.5 Hz; acquired data points, 13.132; and transformation size, 32,000 at room temperature. [^1H-decoupled]^{13}C spectra were acquired with 30000 scans and 31,875 data points. The spectra were integrated and quantified using MestReNova (Master Lab Research).

Fluorescence Recording—Isolated flexor digitorum brevis (FDB) muscle fiber preparations were carried out as described previously (29). FDB muscles were removed, placed in DMEM (Invitrogen) containing 2 mg/ml collagenase A (Roche Applied Science), and incubated under gentle agitation for 3 h at 37 °C. Thereafter, the muscle bundles were transferred to DMEM supplemented with 10% bovine growth serum, 1% penicillin, 1% streptomycin, and 1% glutamine and gently triturated with a polished glass pipette until a significant portion was dissociated to single cells. Myofibers were plated onto ECM-coated (Sigma) glass-bottom dishes (MatTek, Ashland, MA) and allowed to settle to the bottom of the dish.

Whole cell fluorescence changes were detected using an IonOptix fluorescence system (IonOptix, Milton, MA) interfaced with an inverted Zeiss Axiovert 200 microscope equipped with a Neofluar 40× oil immersion objective. Changes in fluores-

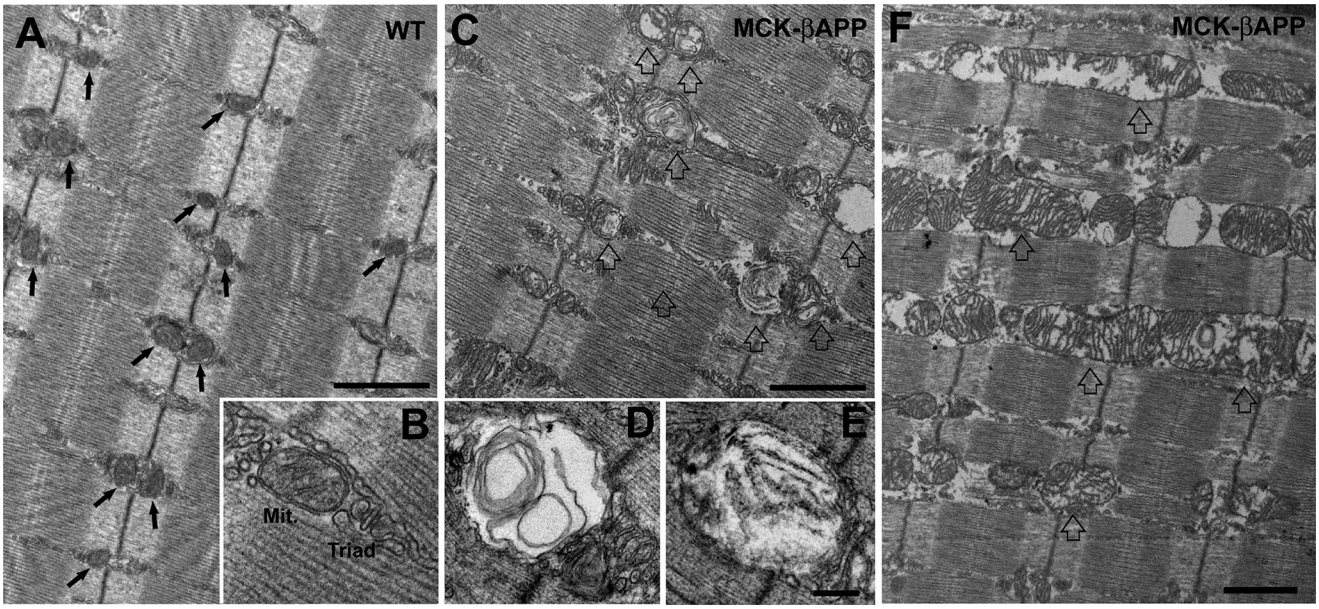

FIGURE 1. **EDL muscle fibers from MCK-βAPP mice showed severe mitochondrial alterations.** *A* and *B*, in WT EDL fibers from 2–3-month-old animals ($n = 3$), mitochondria were primarily located in correspondence to the I band, forming two rows on both sides of each Z line (*A*, *arrows*). Mitochondria (*Mit.*) were located in the close proximity of Ca^{2+} release units or triads (*B*) and presented a healthy appearance (see "Results" for more detail). *C–E*, muscle fibers from 2–3-month-old MCK-βAPP mice ($n = 3$) contained a large number of mitochondria with severely altered morphology (*open arrows*). These mitochondria were usually swollen and contained vacuoles, myelin figures, or lamellar structures surrounded by an almost completely clear matrix (*D* and *E*). *F*, in some fibers mitochondria were abnormally enlarged and formed columns or clusters between myofibrils and/or under the sarcolemma. *Bars*, *A*, *C*, and *F*, 1 μm; *B*, *D*, and *E*, 0.2 μm.

cence were detected by a photo multiplier tube recording signal at 5 kHz. Ca^{2+} transients were elicited by applying suprathreshold rectangular pulses (1-ms duration) through two platinum electrodes placed on opposite sides of the experimental chamber. All of the experiments were conducted at room temperature. The detected changes in fluorescence within each cell were analyzed using IonOptix imaging software (IonOptix, Milton, MA).

Doubled-barreled pH Selective Microelectrode Preparation—The plasma membrane potential (V_m) and intracellular pH were recorded simultaneously using double-barreled microelectrodes that were prepared from thin-walled borosilicate glass capillaries (WPI PB150F-4, Sarasota, FL). Prior to pulling, all of the capillaries were washed with HCl followed by a rinse with distilled water and then dried at 150 °C for 3 h. The capillaries were pulled to make short taper microelectrodes with an outside tip diameter of ~0.6 μm. After being pulled, the double-barreled microelectrodes were heated in a oven (200 °C) for 1 h, and then a small droplet of dimethyldichlorosilane was added into the back of the 1.5-mm (outer diameter) barrel and immediately placed in the oven (200 °C) for another 1 h to polymerize the silane. The V_m barrel (0.75-mm outer diameter) was backfilled with 3 M KCl (tip resistance, 10–15 MΩ), and the was silanized. The pH barrel was filled with neutral proton carrier (ETH-1907; Fluka). All pH-selective microelectrodes were calibrated at room temperature in solutions of known pH and an ionic background mimicking the intracellular milieu before and after the measurements. The pH microelectrodes used in the experiments had a linear dynamic response between pH 9 and 4 and an average slope of 56 mV/pH unit. The potentials from the V_m and the pH barrel were recorded via high impedance amplifier (WPI FD-223, Sarasota, FL), and the V_m potential was electronically subtracted from pH potential to obtain the pH-specific potential, which equivalent to the intracellular pH. Acceptable cellular impalements were characterized by an abrupt negative deflection that remained at a stable value for more than 1 min and that returned to the original base line when the microelectrode was withdrawn. The recordings were conducted at room temperature.

Data Analysis—Statistical analysis was performed using Student's *t* test for two independent populations. Differences were considered to be statistically significant at $p < 0.05$. All of the data are presented as the means ± S.E.

RESULTS

Severe Ultrastructural Alterations in MCK-βAPP Muscle Fibers—Using EDL muscle from 2–3-month-old MCK-βAPP and age-matched WT (control) mice, we performed ultrastructural analysis using EM. Analysis of samples from MCK-βAPP animals revealed that at least 30–40% of muscle fibers exhibited numerous and heterogeneous ultrastructural alterations.

In WT EDL muscle fibers, mitochondria were typically round or slightly oval in shape and located at the I band, on both sides of the Z-line (Fig. 1*A*, *arrows*). In this position, the mitochondria are specifically placed next to Ca^{2+} release units or triads (Fig. 1*B*). This is similar to what has been previously reported for healthy muscle (30). The majority of mitochondria in WT fibers presented a healthy appearance that was characterized by electron-dense matrix, well organized internal cristae, consistent morphology, and an intact outer membrane (as in Fig. 1*B*). Conversely, muscle from MCK-βAPP animals contained numerous fibers with abnormal appearance and many damaged mitochondria (Fig. 1, *C* and *F*). This was rarely observed in WT fibers. The abnormal mitochondria appeared

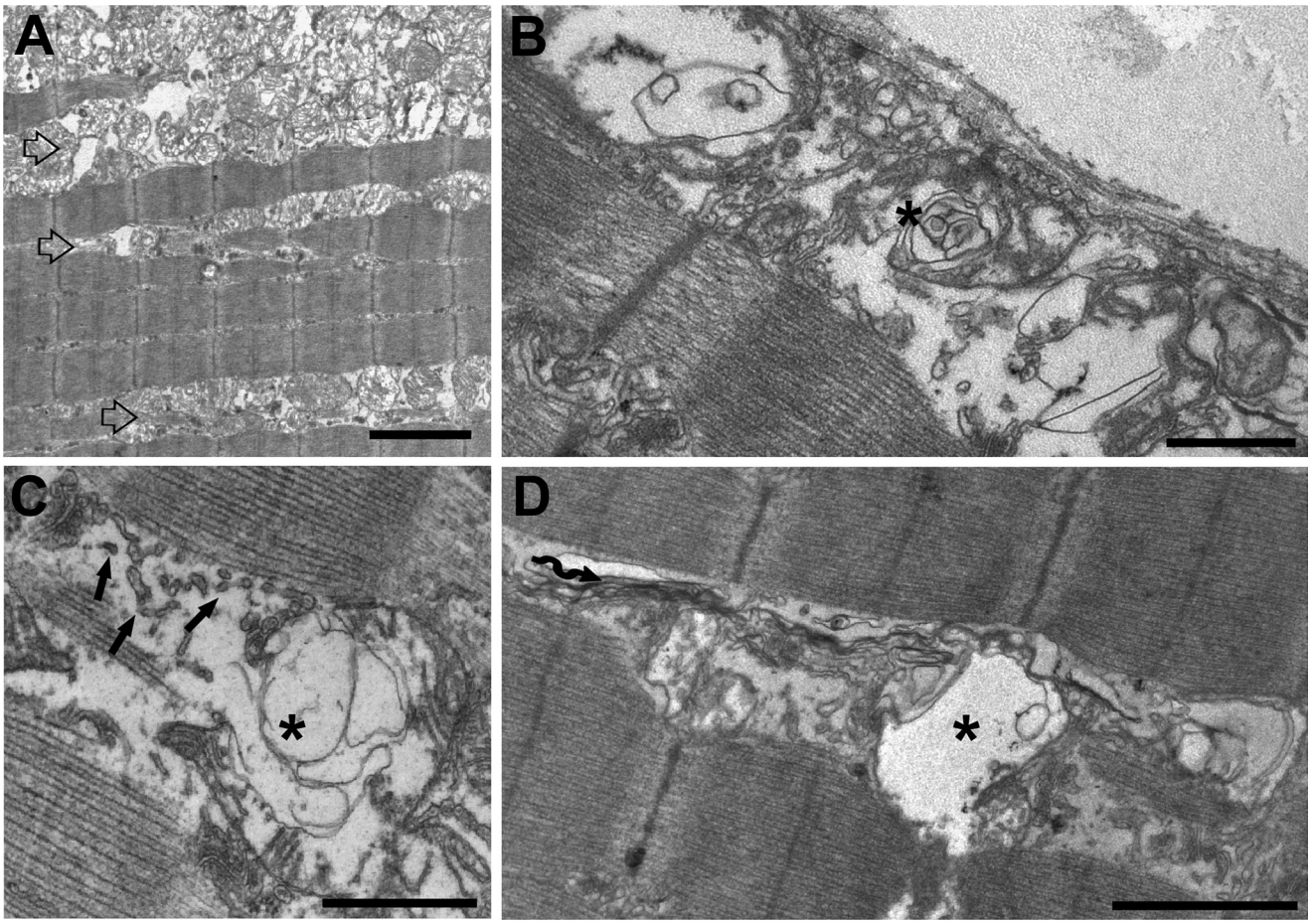

FIGURE 2. **Accumulation of degenerated mitochondria and SR membranes produce areas of vacuolization.** *A*, in some instances, damaged mitochondria formed large clusters that were located either under the sarcolemma or between myofibrils (*open arrows*). *B–D*, mitochondrial degeneration was often associated with SR membrane fragmentation (*C*, *arrows*) and with formation of different size vacuoles (*asterisks*). There were also frequent accumulation of stack-like aggregations of the SR membranes (*wavy arrow*). *Bars*, *A*, 2 μm; *B–D*, 1 μm.

swollen and variable in size and shape (Fig. 1, *C–F*, *open arrows*). Other changes included alterations in the internal cristae that appeared fragmented or, at times, completely missing. In addition, the mitochondrial matrix was translucent and devoid of electron density (Fig. 1*F*). In several instances, mitochondria contained vacuoles, myelin figures, or lamellar structures surrounded by an almost completely clear matrix (Fig. 1, *D* and *E*). Finally, in the more severely affected organelles, the outer membrane was also frequently disrupted. Similar alterations in mitochondrial structure have been described in several human diseases and pathological mouse models (30–32).

Large Areas of Severely Degenerated Mitochondria and SR Membrane Generate Regions of Vacuolization—In some MCK-βAPP, but never in WT fibers, structurally compromised and degenerating mitochondria formed large accumulations (Fig. 2*A*, *open arrows*) that were found either just beneath the sarcolemma or deeper in the cell, between the myofibrils. In these areas, there were also alterations in the SR membranes, which appeared fragmented and compromised (Fig. 2*C*, *arrows*). In these MCK-βAPP fibers, areas with large accumulations of damaged mitochondria coexisted with apparently empty vacuoles (Fig. 2, *B–D*, *asterisks*). These vacuoles closely resemble modifications characteristic of IBM and may represent an early event in the formation of larger vacuoles observed in this disease (33).

Accumulation of Amorphous Electron-dense Material and Formation of Membrane-bound Granular Inclusions—The regions of the cell characterized by accumulation of degenerating mitochondria and vacuolization (Fig. 3, *open arrows*) also contained accumulations of amorphous electron-dense material (Fig. 3, *asterisk*) that was granular in appearance (Figs. 3, *B* and *C*, and 4*A*). There were instances where this material appeared with (Fig. 3*C*, *arrowhead*) and without (Fig. 3*C*, *asterisk*) a membrane envelope. These granular inclusions were also frequently seen in close proximity to mitochondria and triads and in some instances between them (Fig. 4, *B* and *C*).

Altered TCA Cycle in Aβ-affected Muscle—To correlate the effects of intramyofiber accumulation of Aβ with potential alterations in the mitochondrial TCA cycle activity, we performed parallel ELISA and high frequency [^{1}H-decoupled]^{13}C NMR spectroscopy with the muscle tissue from the 2-month-old animals. Because MCK-βAPP mice are engineered to express human APP transgene, we performed ELISA specifically for human $A\beta_{1-40}$ and $A\beta_{1-42}$ to determine whether toxic Aβ fragments are present at an early age in the muscle of MCK-βAPP mice. No differences in the levels of $A\beta_{1-42}$ were

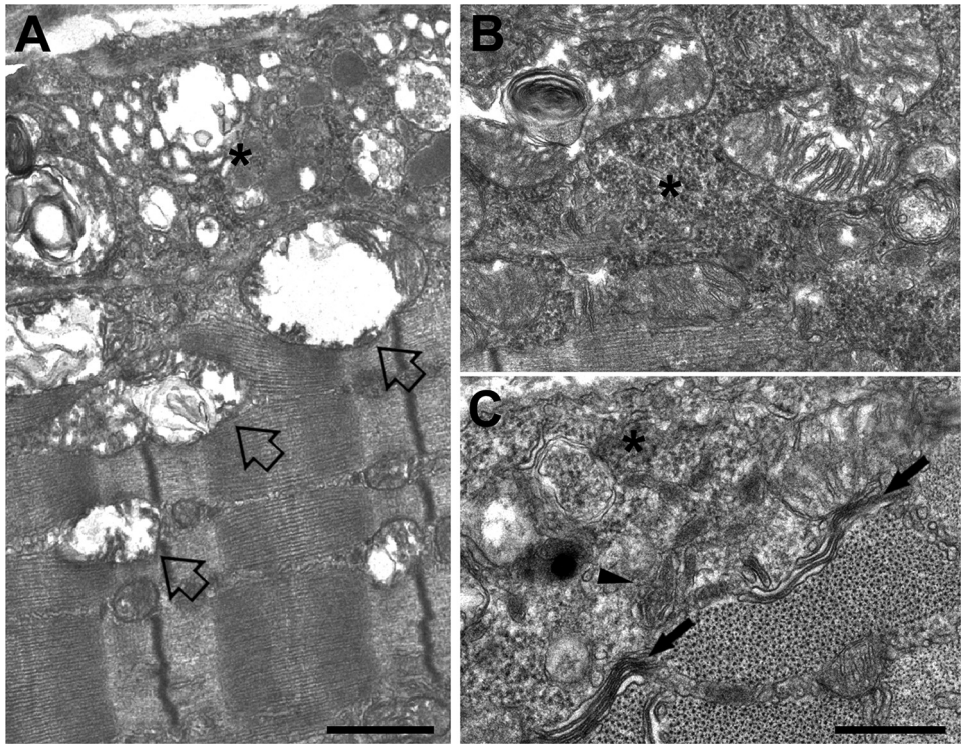

FIGURE 3. **Accumulation of amorphous materials and membrane bound inclusions.** *A*, regions of the cell characterized by accumulation of degenerating mitochondria and vacuolization (*open arrows*) also contained accumulations of amorphous electron-dense material (*asterisks*). *B* and *C*, the electron-dense material was granular in appearance and was observed either with (*C*, *arrowhead*) or without (*C*, *asterisk*) a membrane envelope. In certain MCK-βAPP fibers, stack-like aggregations of the SR membranes were also observed (*wavy arrows*). *Bars*, *A*, 1 μm; *B* and *C*, 0.5 μm.

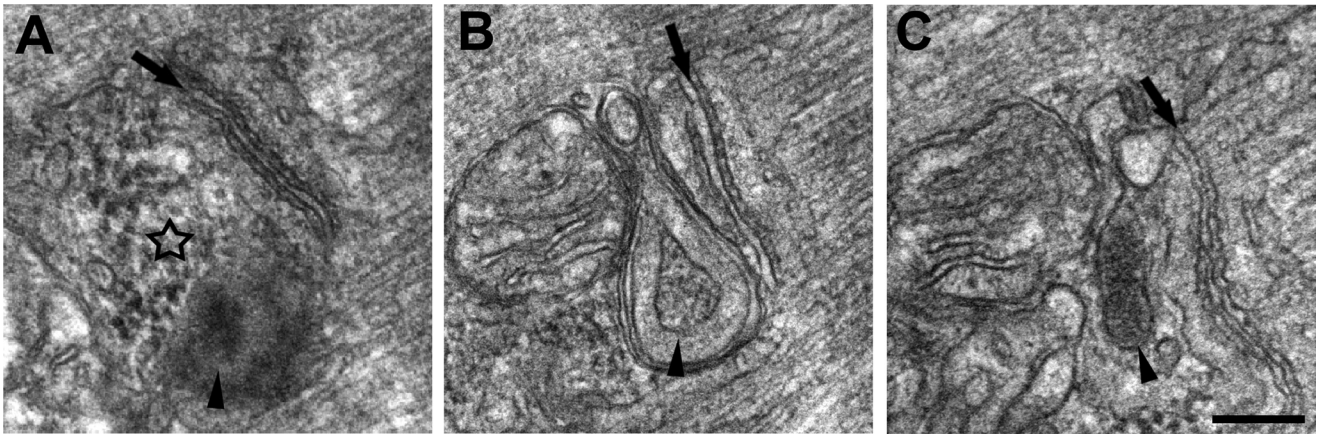

FIGURE 4. **Accumulation of amorphous electron-dense material and formation of membrane-bound granular inclusions in proximity of triads and mitochondria of MCK-βAPP muscle fibers.** Electron-dense bodies of granular electron-dense material were found in MCK-βAPP muscle fibers, often in proximity of triads and mitochondria. *Arrows* mark the central elements of triads, the T-tubule, whereas the *star* in *A* points to an accumulation of electron-dense material, which is not yet as dense and not enclosed in a membrane as those indicated by *arrowheads* in *B* and *C*. *Bar*, *A–C*, 0.2 μm.

detected between the genotypes. However, the levels of $A\beta_{1-40}$ were significantly greater in MCK-βAPP compared with control mice (Fig. 5*A*). To determine whether there is a correlation between Aβ accumulation and mitochondrial activity at this early age, mice were injected with [^{13}C]pyruvate, and muscle tissue was collected 45 min after injection. With this approach, ^{13}C served as a label for succinate, a TCA cycle intermediate. NMR analysis of 5% perchloric acid muscle extracts showed a 3-fold reduction in the level of ^{13}C labeling of succinate C2/C3 (Fig. 5*B*) and a 4-fold reduction in its total pool size (Fig. 5*C*), indicating a diminished activity of the mitochondrial TCA cycle. To further investigate the possibility of reduced TCA cycle activity, we determined the levels of glutamate, a by-product of the TCA cycle metabolism. Our results revealed a significant decrease of ^{13}C flux into glutamate C4 (33%) and C2 (27%) consistent with a decrease (34%) in total glutamate levels. This further indicates that TCA cycle metabolism is compromised at an early age in the muscle of MCK-βAPP mice. Because the reduction in mitochondrial metabolism suggests a possible switch to anaerobic metabolism, which is expected to lead to increased accumulation of lactic acid, we also compared the levels of lactate between control and Aβ-affected muscle. Flux of the ^{13}C label into lactate C3 was significantly increased (94%) in MCK-βAPP compared with control mice. This was congru-

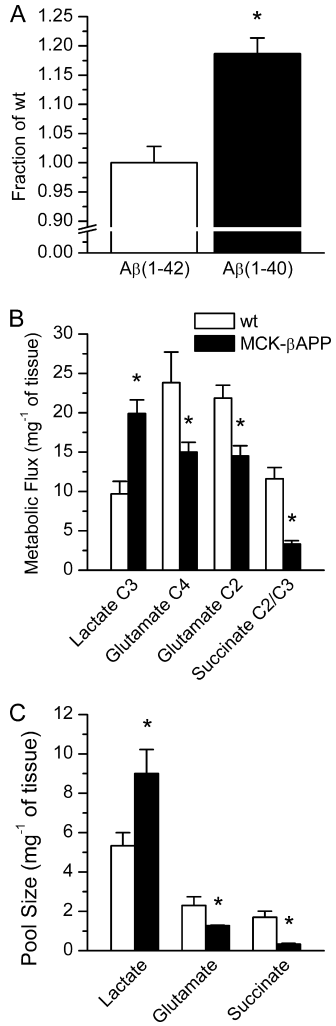

FIGURE 5. **Increased levels of $A\beta_{1-40}$ and altered TCA cycle metabolism in MCK-βAPP muscle.** *A*, ELISA measurement of the levels of human $A\beta_{1-42}$ and $A\beta_{1-40}$ in hamstring muscle extracts from MCK-βAPP mice in 30% formic acid. *B*, metabolic flux of ^{13}C label from 1-[^{13}C]pyruvate into isotopomers of lactate at C3, glutamate at C4 and C2, and succinate at C2/C3 as measured by [^{1}H-decoupled]^{13}C NMR spectroscopy. *C*, total metabolite pool size of lactate, glutamate, and succinate as measured by [^{13}C-decoupled]^{1}H NMR spectroscopy ($n = 4$; *, $p < 0.05$, *t* test).

ent with an increase (70%) in total lactate levels and further indicates an impairment of mitochondrial TCA cycle activity concurrent with the intracellular accumulation of Aβ.

Increased ROS Production and Partial Loss of $\Delta\Psi_m$ in β-Amyloid Affected Muscle Cells—Because cytoplasmic [Ca^{2+}] ([Ca^{2+}]$_i$) is augmented in MCK-βAPP muscle cells (17, 29), a consequent progressive increase in mitochondrial Ca^{2+} accumulation could result in increased production of ROS as well as increased frequency of PT pore opening ultimately, leading to a loss of the mitochondrial membrane potential ($\Delta\Psi_m$).

To compare the ROS production between healthy and Aβ-affected muscle, enzymatically dissociated FDB fibers from 2-month-old WT and MCK-βAPP mice were loaded with the ROS probe, 5-(and 6-)chloromethyl-2′,7′-dichlorodihydrofluorescein diacetate. Upon cleavage of the acetate groups by intracellular esterases and oxidation, the nonfluorescent 2′,7′-dichlorodihydrofluorescein diacetate is converted to the highly fluorescent 2′,7′-dichlorofluorescein (DCF). As demonstrated in Fig. 6, the rate of DCF oxidation was much greater in resting MCK-βAPP fibers compared with the WT cells, suggesting that Aβ-producing cells were generating a greater amount of ROS.

Mitochondrial membrane potential was monitored in isolated FDB fibers loaded with TMRE, a fluorescent indicator whose accumulation in mitochondria is driven by $\Delta\Psi_m$. For mitochondrial localization, fibers were simultaneously loaded with MitoTracker Green FM (MTG), which accumulates within mitochondria regardless of $\Delta\Psi_m$. The distribution patterns for MitoTracker Green and TMRE were uniform across the genotypes (Fig. 6*C*). However, further analysis of TMRE fluorescence within individual mitochondria showed that MCK-βAPP cells contained a large population of mitochondria that exhibited diminished TMRE fluorescence (Fig. 6*D*) suggesting that these organelles were partially depolarized. The partial loss of $\Delta\Psi_m$ appears to be an age-dependent phenomenon because muscle cells from older animals (6 months old), which exhibit greater dysregulation of cytoplasmic Ca^{2+} (17), contained an even larger fraction of depolarized mitochondria.

Acidification of Cytoplasm and Plasma Membrane Depolarization—The increased level of lactate shown in Fig. 5 is expected to cause acidification of the cytoplasm. The combination of acidic pH and increased ROS production can lead to excessive lipid peroxidation and subsequent depolarization of the plasma membrane. Our previous results demonstrate that intramyofiber accumulation of Aβ results in partial depolarization of the plasma membrane (17, 29). Using ion selective microelectrodes, we simultaneously measured pH and V_m in WT and MCK-βAPP muscle fibers (Fig. 7). Consistent with previous observations, MCK-βAPP myofibers exhibited a partially depolarized plasma membrane in comparison with the WT fibers (Fig. 7*A*). The pH in the same cells was also more acidic compared with the controls (Fig. 7*B*). To determine whether these phenomena were driven by alterations in the mitochondrial Ca^{2+} homeostasis, the cells were treated for 24 h with Ru360 (1 nM), a highly selective blocker of the mitochondrial Ca^{2+} uniporter (34). These treatments resulted in partial reversal of changes in V_m (Fig. 7*A*) and complete reversal of changes in pH (Fig. 7*B*) in MCK-βAPP cells without affecting these parameters in the control cells. These results suggest that functional modifications of mitochondria and subsequent cytoplasmic alterations are potentially mediated by Ca^{2+} transport through the mitochondrial Ca^{2+} uniporter and subsequent mitochondrial Ca^{2+} overload.

Because ryanodine receptor Ca^{2+} release channels (RyR) contain reactive thiol residues, the functional state of these channels is modulated by the cellular redox state. Based on these factors, it is feasible that alterations in depolarization evoked Ca^{2+} release previously reported in MCK-βAPP muscle (17, 29) arise, in part, from altered redox state via augmented mitochondrial ROS production and decreased cytoplasmic pH. To assess whether oxidation of RyRs is responsible for reduction in Ca^{2+} release from the SR, MCK-βAPP cells were treated with glutathione (GSH), a potent antioxidant. A 24-h treatment with GSH (5 mM) increased the peak amplitude of single square electrical pulse-elicited Ca^{2+} release in the MCK-βAPP muscle fibers (Fig. 7, *C* and *D*) without affecting the peak amplitudes of Ca^{2+} transients in the WT cells (not shown). Together, these

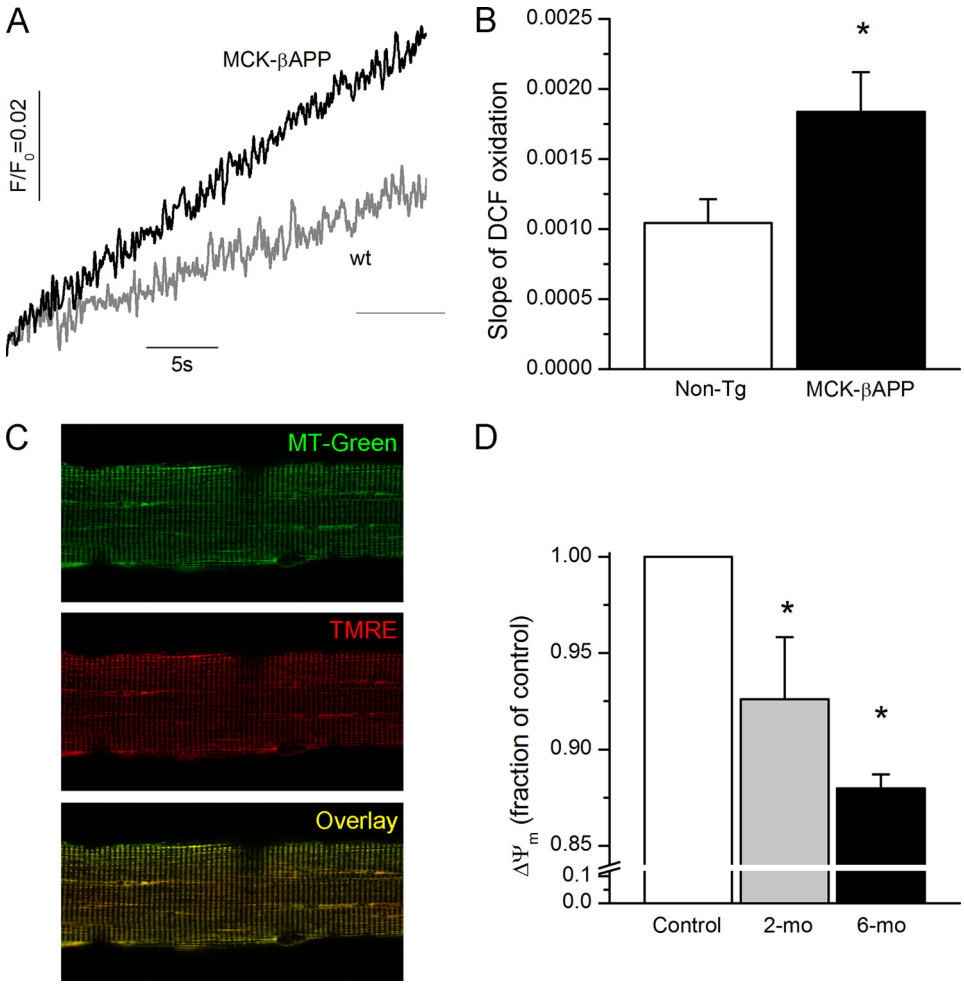

FIGURE 6. **Increased rate of ROS production and reduced $\Delta\Psi_m$ in MCK-βAPP muscle fibers.** *A*, temporal change in DCF fluorescence in WT and MCK-βAPP muscle fibers. *B*, rate of change (slope) in DCF fluorescence in WT ($n = 14$) and MCK-βAPP ($n = 16$) muscle fibers. *C*, confocal images of FDB muscle fibers loaded with MitoTracker Green (*MT-Green*, *top panel*) and TMRE (*middle panel*). The *bottom panel* presents a merged image of MitoTracker Green and TMRE fluorescence. *D*, mean intensity of TMRE fluorescence of individual mitochondria presented as fraction of control in 2-month-old (*2-mo*) WT ($n_{mito} = 626$) and MCK-βAPP ($n_{mito} = 796$) and 6-month-old (*6-mo*) WT ($n_{mito} = 1127$) and MCK-βAPP ($n_{mito} = 1288$) muscle fibers. *, $p < 0.05$ (*t* test).

results demonstrate that alterations in Ca^{2+} release in MCK-βAPP muscle were partly due to oxidation of RyRs.

DISCUSSION

The main goal of the current study was to determine the effects of intracellular Aβ accumulation on mitochondrial structure and function in skeletal muscle. Our results demonstrate that severe structural alterations in mitochondria and other subsarcolemmal organelles, as well as disruption of TCA cycle activity, coincide with accumulation of Aβ in skeletal muscle. This study utilized MCK-βAPP transgenic mice that accumulate Aβ specifically in skeletal muscle and reportedly exhibit age-dependent appearance of numerous features analogous to those observed in IBM such as intracellular inclusions, angulated fibers, inflammation, and deficits in motor performance. However, none of the myopathic features have been previously reported in the MCK-βAPP mice at ages chosen for this study (15). We specifically chose to study young MCK-APP mice to explore the effects of the Aβ prior to the appearance of IBM disease features.

The alterations in mitochondrial structure and function were likely caused by the initial overexpression of the APP and accumulation of its proteolytic fragments. Our results point out that at the current stage of the disease progression, MCK-βAPP muscle predominantly accumulates the $A\beta_{1-40}$ species of β-amyloid rather than $A\beta_{1-42}$, which is considered to be the more toxic species. Although the specific effects of these peptides on mitochondria are still under investigation, Aβ has been demonstrated to accumulate into this organelle and destabilize its membrane properties (35, 36). Deleterious effects of Aβ on the mitochondrial function include reduced cytochrome *c* oxidase activity (35, 37) caused by inhibition of its gene expression (37), decreased respiration and ATP synthesis, and cytochrome *c* release (35, 38).

Despite the existence of many fibers presenting normal ultrastructure in the MCK-βAPP muscle, a significant number of fibers showed compromised mitochondrial apparatus. These alterations are exemplified by a large number of mitochondria with altered morphological internal cristae, suggesting that these organelles were at varying stages of degeneration. Furthermore, these degenerated mitochondria often accumulated in large clusters under the sarcolemma or, less frequently, between myofibrils. Interestingly, under high magnification,

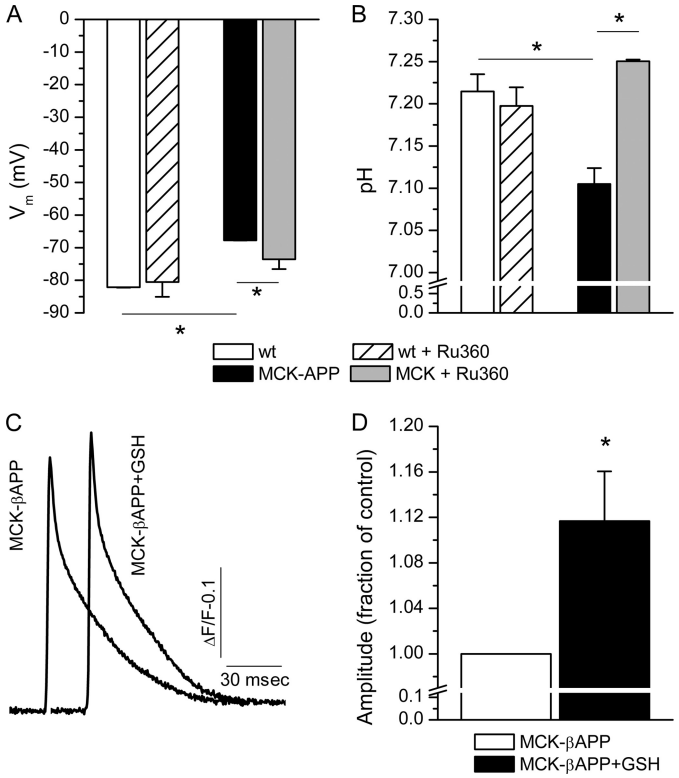

FIGURE 7. **Alterations in V_m and pH in MCK-βAPP muscle fibers.** *A*, recording of resting membrane potential (V_m) with microelectrodes in 2-month-old WT ($n = 3$) and MCK-βAPP ($n = 4$) muscle fibers before and after 24 h of treatment with Ru360 (1 nM). MCK-βAPP cells exhibited depolarized plasma membrane. This alteration could be partially reversed by Ru360 treatment. *B*, recording of intracellular pH with microelectrodes in the same WT and MCK-βAPP muscle fibers as in *A* before and after 24 h of treatment with Ru360 (1 nM). MCK-βAPP cell exhibited reduced pH compared with WT cells. Treatment with Ru360 had no effect on the WT cell but increased pH to near normal level. *C*, mean MagFluo-4 fluorescence transient from untreated ($n = 17$) and GSH-treated ($n = 21$, 5 mM for 24 h) MCK-βAPP muscle fibers. Ca^{2+} transients were elicited by 1-ms single square electrical pulses. *D*, peak amplitude of Ca^{2+} release in untreated and GSH treated MCK-βAPP muscle fibers. GSH treatment increased peak amplitudes of Ca^{2+} transients in DJ-1 null cells. *, $p < 0.05$ (*t* test).

areas of mitochondrial clusters appear to be analogous to what has been described in vacuolated fibers of IBM patients (39). In these areas, there are several additional characteristic features of Aβ-accumulating fibers that include the presence of what appear to be autophagic vacuoles, myelin bodies, membrane whorls, and granular and filamentous membrane-bound inclusions. The EM data also show mitochondrial impairment and ultrastructural modifications that are consistent with previous findings, which demonstrated alterations in lysosomal enzymes and up-regulation of autophagic activity in IBM and cultured human muscle fibers, thus collectively suggesting that IBM muscle may have autophagic defects (40). The results presented here point to a possibility that the mitochondrial impairments and ultrastructural modifications could be mediated by autophagic removal of defective mitochondria via mitophagy in MCK-βAPP muscle. In addition to mitochondrial alterations, we also observed degeneration of the SR membranes, which could contribute to the previously described impairment in the excitation-contraction coupling mechanism (17, 29). All of the above described alterations in the MCK-βAPP muscle are likely to have a negative impact on muscle contractility and may contribute to the development of muscle weakness.

The disruption of mitochondrial ultrastucture can potentially account for the diminished TCA cycle activity and the reduced $\Delta\Psi_m$ that were observed in MCK-βAPP muscle. Mitochondrial abnormalities have been described in IBM (12, 13). Similarly, mitochondrial alterations are found in a mouse model for amyotrophic lateral sclerosis (32) and in core-like myopathies such as the malignant hyperthermia (MH) (41). Interestingly, in each case, these alterations have been associated with a high level of oxidative stress.

In MCK-βAPP mice, the functional consequences of altered mitochondrial activity is manifested by the reduced production of the TCA cycle intermediates and by-products, increased ROS generation, and increased lactic acid production, which at least partially contributed to a more acidic cytoplasm. The increase in the lactic acid accumulation reflects the fact that there is a shift in the equilibrium between the aerobic and the anaerobic glucose metabolism. The reduced TCA cycle activity is expected to lead to a reduced mitochondrial generation of ATP. However, because MCK-βAPP animals do not exhibit muscle weakness at this age (16), it seems that a potential reduction in ATP levels at this early stage of the disease progression is not sufficient to appreciably affect ATP-dependent processes. Nevertheless, the progressive nature of Aβ accumulation will likely lead to greater mitochondrial dysfunction that could ultimately result in a substantial reduction of cellular ATP levels, thus influencing the muscle strength and other ATP-dependent signaling pathways.

The acidification of the cytoplasm and enhanced ROS production in resting Aβ-affected myofibers could further result in altered cellular Ca^{2+} handling. Oxidation of the reactive thiols of the RyR1 is known to increase channel activity. This is partly due to altered sensitivity of the channel to ATP, Ca^{2+}, and Mg^{2+} and modified interactions of RyRs with the auxiliary proteins (42, 43). Our previous investigation has shown that Aβ can also directly increase RyR channel activity (29). The current results suggest that oxidation of the RyRs may be partially responsible for the reduced SR Ca^{2+} release in the MCK-βAPP muscle. An acidic cytoplasm may affect the rate of Ca^{2+} uptake into SR by reducing the affinity of the SR Ca^{2+} ATPase (SERCA) pump to Ca^{2+} (44, 45). Although we did not observe any changes in Ca^{2+} reuptake parameters (not shown), which in part reflect Ca^{2+} uptake by the SERCA, in the mice at ages chosen for this study, the rate of Ca^{2+} uptake is significantly slower in the older MCK-βAPP mice (29). Thus, a cumulative effect of RyR oxidation, enhanced RyR channel activity caused by modulation by Aβ and reduced activity of the SERCA, could be responsible for increased $[Ca^{2+}]_i$ at rest and diminished excitation-contraction coupling in Aβ affected cells in the later stages of disease progression.

The precise mechanism of the functional interplay between Aβ accumulation, mitochondrial dysfunction, and altered Ca^{2+} remains to be determined. However, based on the currently available information, we put forth the following working model for the effects of Aβ accumulation on mitochondrial function, intracellular Ca^{2+} handling, and development of muscle weakness in IBM (Fig. 8). Studies have shown that Aβ

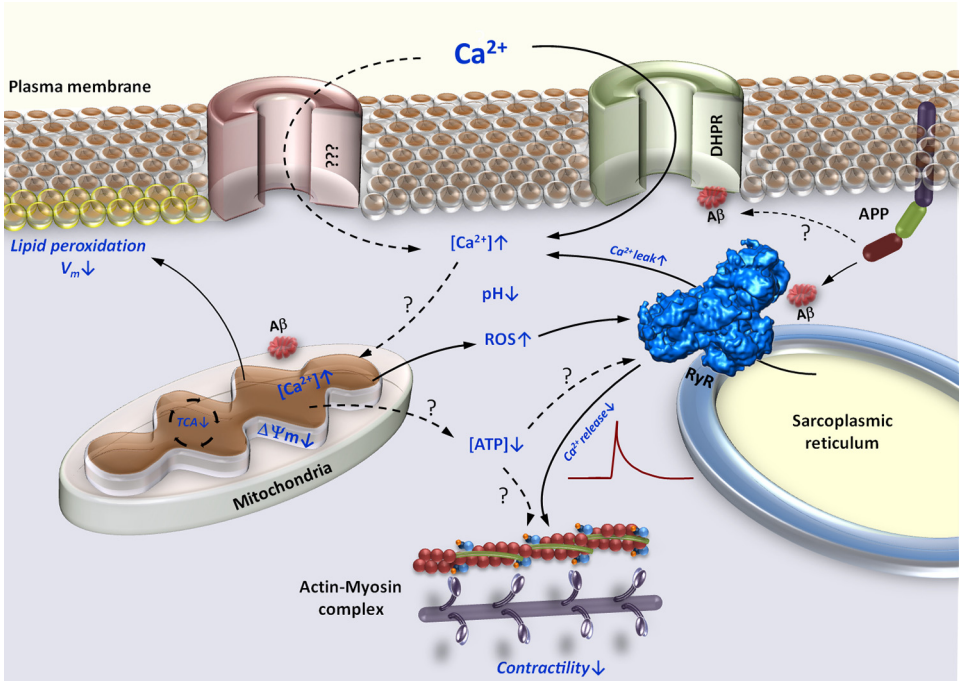

FIGURE 8. **Proposed model of β-amyloid mediated muscle dysfunction in IBM.** Increased expression of APP and accumulation of its proteolytic Aβ fragments affects numerous intracellular regulatory complexes. Modulation of the intracellular Ca^{2+} release channels (RyR), dihydropyridine receptors (DHPR) and possibly other surface membrane Ca^{2+} channels leads to Ca^{2+} efflux and influx, respectively, which contribute to augmentation of the resting cytoplasmic Ca^{2+} concentration ($[Ca^{2+}]_i$). Aβ accumulation also leads to decreased Ca^{2+} release by RyRs. Augmented $[Ca^{2+}]_i$ together with modification of mitochondrial function by Aβ lead to enhanced Ca^{2+} flux into the mitochondrial matrix and subsequent mitochondrial Ca^{2+} overload. Mitochondrial Ca^{2+} overload promotes enhanced generation of ROS, mitochondrial permeability transition pore complex opening, and disruption of $\Delta\Psi_m$. Diminished $\Delta\Psi_m$ results in inefficient TCA cycle and reduction in mitochondrial ATP production. Increased ROS production in combination with acidic cytoplasm promotes lipid peroxidation, further increase in $[Ca^{2+}]_i$, and reduction in Ca^{2+} release from the SR through modulation of the RyRs. All of these events combine to lead to diminished muscle contractility. *Solid arrows* represent observed, whereas *dashed arrows* represent unconfirmed effects of Aβ.

accumulations can lead to modulation of L-type Ca^{2+} channel properties (46, 47). Whether these effects result from direct modification of these channels by Aβ or whether this modulation is indirect remains to be determined. There is recent evidence that Aβ can interact with the β subunit of $Ca_V1.2$ and $Ca_V1.3$ L-type Ca^{2+} channels (48). Additional studies need to be carried out to determine whether this interaction takes place between Aβ and $Ca_V1.1$ in the skeletal muscle. Studies have shown that Aβ-accumulating cells exhibit a nifedipine-sensitive augmentation of the cytoplasmic $[Ca^{2+}]$ in muscle (17) and neurons (49), thus suggesting a contribution of L-type Ca^{2+} channels to changes in cytoplasmic Ca^{2+} handling.

It has been demonstrated that both the extracellular and the intracellular compartments contribute to the augmented $[Ca^{2+}]$ in MCK-APP muscle (17). It is likely that RyR-mediated Ca^{2+} efflux could be a major intracellular contributor to this phenomenon. Direct binding of Aβ to RyR has not been demonstrated; however, previous investigations have shown that Aβ can effectively modulate RyR function when these channels are reconstituted in the planar lipid bilayers and in SR vesicles prepared from the skeletal muscle (29).

Concurrently with alterations in the cytoplasmic $[Ca^{2+}]$, Aβ can accumulate within the mitochondria (35, 36) and possibly lower the threshold for activation of the mitochondrial Ca^{2+} transporters, such as the Ca^{2+} uniporter, and lead to mitochondrial Ca^{2+} overload. Effects of mitochondrial Ca^{2+} overload include, among others, swelling of the mitochondria and activation of the mitochondrial permeability transition pore complex that leads to the loss of the $\Delta\Psi_m$ and a burst of ROS. Similar features are observed in MCK-βAPP muscle and are presented in this study. The increased mitochondrial permeability transition pore complex opening could affect the plasma membrane integrity,which is manifested by the lipid peroxidation and depolarization of plasmalemma. Increased ROS production could also enhance Ca^{2+} leak from the SR. The diminished cellular ATP levels that likely arise from mitochondrial impairment can later lead to a reduction of the stimulated SR Ca^{2+} release and affect Ca^{2+} sequestration by the SR after muscle contraction. Based on this hypothetical model, it is conceivable that Aβ can be a catalyst that initiates a vicious cycle whereby disrupted Ca^{2+} homeostasis exerts a negative effect on the mitochondrial function and vice versa in the pathogenesis of IBM.

In summary, the present results demonstrate that Aβ accumulation within skeletal muscle leads to considerable alterations in mitochondrial structure and function that precede other reported aspects of IBM in the MCK-βAPP transgenic mice. The functional interplay between the disrupted cytoplasmic Ca^{2+} handling and diminished mitochondrial function in Aβ-affected muscle could potentially serve as therapeutic target for the treatment of IBM and other Aβ-mediated disorders.

Acknowledgment—We thank the Drug Discovery Unit at Georgetown University for the use of the NMR equipment.

REFERENCES

1. Askanas, V., Serratrice, G., and Engel, W. K. (1998) *Inclusion-Body Myositis and Myopathies*, Cambridge University Press, Cambridge
2. Askanas, V., Alvarez, R. B., and Engel, W. K. (1993) β-Amyloid precursor epitopes in muscle fibers of inclusion body myositis. *Ann. Neurol.* **34,** 551–560
3. Askanas, V., Serdaroglu, P., Engel, W. K., and Alvarez, R. B. (1991) Immunolocalization of ubiquitin in muscle biopsies of patients with inclusion body myositis and oculopharyngeal muscular dystrophy. *Neurosci. Lett.* **130,** 73–76
4. Askanas, V., Engel, W. K., Bilak, M., Alvarez, R. B., and Selkoe, D. J. (1994) Twisted tubulofilaments of inclusion body myositis muscle resemble paired helical filaments of Alzheimer brain and contain hyperphosphorylated tau. *Am. J. Pathol.* **144,** 177–187
5. Fidziańska, A., and Glinka, Z. (2006) Rimmed vacuoles with β-amyloid and Tau protein deposits in the muscle of children with hereditary myopathy. *Acta Neuropathol.* **112,** 185–193
6. Schmidt, J., Barthel, K., Wrede, A., Salajegheh, M., Bähr, M., and Dalakas, M. C. (2008) Interrelation of inflammation and APP in sIBM. IL-1β induces accumulation of β-amyloid in skeletal muscle. *Brain* **131,** 1228–1240
7. Vattemi, G., Nogalska, A., King Engel, W., D'Agostino, C., Checler, F., and Askanas, V. (2009) Amyloid-β42 is preferentially accumulated in muscle fibers of patients with sporadic inclusion-body myositis. *Acta Neuropathol.* **117,** 569–574
8. Nogalska, A., D'Agostino, C., Engel, W. K., Klein, W. L., and Askanas, V. (2010) Novel demonstration of amyloid-β oligomers in sporadic inclusion-body myositis muscle fibers. *Acta Neuropathol.* **120,** 661–666
9. Askanas, V., Engel, W. K., and Alvarez, R. B. (1992) Light and electron microscopic localization of β-amyloid protein in muscle biopsies of patients with inclusion-body myositis. *Am. J. Pathol.* **141,** 31–36
10. Askanas, V., McFerrin, J., Alvarez, R. B., Baqué, S., and Engel, W. K. (1997) βAPP gene transfer into cultured human muscle induces inclusion-body myositis aspects. *Neuroreport* **8,** 2155–2158
11. Askanas, V., McFerrin, J., Baqué, S., Alvarez, R. B., Sarkozi, E., and Engel, W. K. (1996) Transfer of β-amyloid precursor protein gene using adenovirus vector causes mitochondrial abnormalities in cultured normal human muscle. *Proc. Natl. Acad. Sci. U.S.A.* **93,** 1314–1319
12. Oldfors, A., Moslemi, A. R., Jonasson, L., Ohlsson, M., Kollberg, G., and Lindberg, C. (2006) Mitochondrial abnormalities in inclusion-body myositis. *Neurology* **66,** S49–55
13. Horvath, R., Fu, K., Johns, T., Genge, A., Karpati, G., and Shoubridge, E. A. (1998) Characterization of the mitochondrial DNA abnormalities in the skeletal muscle of patients with inclusion body myositis. *J. Neuropathol. Exp. Neurol.* **57,** 396–403
14. Sugarman, M. C., Kitazawa, M., Baker, M., Caiozzo, V. J., Querfurth, H. W., and LaFerla, F. M. (2006) Pathogenic accumulation of APP in fast twitch muscle of IBM patients and a transgenic model. *Neurobiol. Aging* **27,** 423–432
15. Sugarman, M. C., Yamasaki, T. R., Oddo, S., Echegoyen, J. C., Murphy, M. P., Golde, T. E., Jannatipour, M., Leissring, M. A., and LaFerla, F. M. (2002) Inclusion body myositis-like phenotype induced by transgenic overexpression of βAPP in skeletal muscle. *Proc. Natl. Acad. Sci. U.S.A.* **99,** 6334–6339
16. Moussa, C. E., Fu, Q., Kumar, P., Shtifman, A., Lopez, J. R., Allen, P. D., LaFerla, F., Weinberg, D., Magrane, J., Aprahamian, T., Walsh, K., Rosen, K. M., and Querfurth, H. W. (2006) Transgenic expression of β-APP in fast-twitch skeletal muscle leads to calcium dyshomeostasis and IBM-like pathology. *FASEB J.* **20,** 2165–2167
17. Lopez, J. R., and Shtifman, A. (2010) Intracellular β-amyloid accumulation leads to age-dependent progression of Ca^{2+} dysregulation in skeletal muscle. *Muscle Nerve* **42,** 731–738
18. Brookes, P. S., Yoon, Y., Robotham, J. L., Anders, M. W., and Sheu, S. S. (2004) Calcium, ATP, and ROS. A mitochondrial love-hate triangle. *Am. J. Physiol. Cell Physiol.* **287,** C817–C833
19. Denton, R. M., and McCormack, J. G. (1985) Physiological role of Ca^{2+} transport by mitochondria. *Nature* **315,** 635
20. Denton, R. M., and McCormack, J. G. (1986) The calcium sensitive dehydrogenases of vertebrate mitochondria. *Cell Calcium* **7,** 377–386
21. Wang, W., Fang, H., Groom, L., Cheng, A., Zhang, W., Liu, J., Wang, X., Li, K., Han, P., Zheng, M., Yin, J., Wang, W., Mattson, M. P., Kao, J. P., Lakatta, E. G., Sheu, S. S., Ouyang, K., Chen, J., Dirksen, R. T., and Cheng, H. (2008) Superoxide flashes in single mitochondria. *Cell* **134,** 279–290
22. Chen, Q., Chai, Y. C., Mazumder, S., Jiang, C., Macklis, R. M., Chisolm, G. M., and Almasan, A. (2003) The late increase in intracellular free radical oxygen species during apoptosis is associated with cytochrome c release, caspase activation, and mitochondrial dysfunction. *Cell Death Differ* **10,** 323–334
23. Casley, C. S., Canevari, L., Land, J. M., Clark, J. B., and Sharpe, M. A. (2002) β-Amyloid inhibits integrated mitochondrial respiration and key enzyme activities. *J. Neurochem.* **80,** 91–100
24. Casley, C. S., Land, J. M., Sharpe, M. A., Clark, J. B., Duchen, M. R., and Canevari, L. (2002) β-Amyloid fragment 25–35 causes mitochondrial dysfunction in primary cortical neurons. *Neurobiol. Dis.* **10,** 258–267
25. Eckert, A., Hauptmann, S., Scherping, I., Rhein, V., Müller-Spahn, F., Götz, J., and Müller, W. E. (2008) Soluble β-amyloid leads to mitochondrial defects in amyloid precursor protein and Tau transgenic mice. *Neurodegener Dis.* **5,** 157–159
26. Grant, S. M., Shankar, S. L., Chalmers-Redman, R. M., Tatton, W. G., Szyf, M., and Cuello, A. C. (1999) Mitochondrial abnormalities in neuroectodermal cells stably expressing human amyloid precursor protein (hAPP751). *Neuroreport* **10,** 41–46
27. Keil, U., Bonert, A., Marques, C. A., Scherping, I., Weyermann, J., Strosznajder, J. B., Müller-Spahn, F., Haass, C., Czech, C., Pradier, L., Müller, W. E., and Eckert, A. (2004) Amyloid β-induced changes in nitric oxide production and mitochondrial activity lead to apoptosis. *J. Biol. Chem.* **279,** 50310–50320
28. Pereira, C., Santos, M. S., and Oliveira, C. (1998) Mitochondrial function impairment induced by amyloid β-peptide on PC12 cells. *Neuroreport* **9,** 1749–1755
29. Shtifman, A., Ward, C. W., Laver, D. R., Bannister, M. L., Lopez, J. R., Kitazawa, M., LaFerla, F. M., Ikemoto, N., and Querfurth, H. W. (2010) Amyloid-β protein impairs Ca^{2+} release and contractility in skeletal muscle. *Neurobiol. Aging* **31,** 2080–2090
30. Boncompagni, S., Rossi, A. E., Micaroni, M., Beznoussenko, G. V., Polishchuk, R. S., Dirksen, R. T., and Protasi, F. (2009) Mitochondria are linked to calcium stores in striated muscle by developmentally regulated tethering structures. *Mol. Biol. Cell* **20,** 1058–1067
31. Chung, M. J., and Suh, Y. L. (2002) Ultrastructural changes of mitochondria in the skeletal muscle of patients with amyotrophic lateral sclerosis. *Ultrastruct. Pathol.* **26,** 3–7
32. Dobrowolny, G., Aucello, M., Rizzuto, E., Beccafico, S., Mammucari, C., Bonconpagni, S., Belia, S., Wannenes, F., Nicoletti, C., Del Prete, Z., Rosenthal, N., Molinaro, M., Protasi, F., Fanò, G., Sandri, M., and Musarò, A. (2008) Skeletal muscle is a primary target of SOD1G93A-mediated toxicity. *Cell Metab.* **8,** 425–436
33. Yunis, E. J., and Samaha, F. J. (1971) Inclusion body myositis. *Lab. Invest.* **25,** 240–248
34. Matlib, M. A., Zhou, Z., Knight, S., Ahmed, S., Choi, K. M., Krause-Bauer, J., Phillips, R., Altschuld, R., Katsube, Y., Sperelakis, N., and Bers, D. M. (1998) Oxygen-bridged dinuclear ruthenium amine complex specifically inhibits Ca^{2+} uptake into mitochondria *in vitro* and *in situ* in single cardiac myocytes. *J. Biol. Chem.* **273,** 10223–10231
35. Aleardi, A. M., Benard, G., Augereau, O., Malgat, M., Talbot, J. C., Mazat, J. P., Letellier, T., Dachary-Prigent, J., Solaini, G. C., and Rossignol, R. (2005) Gradual alteration of mitochondrial structure and function by β-amyloids. Importance of membrane viscosity changes, energy deprivation, reactive oxygen species production, and cytochrome c release. *J. Bioenerg. Biomembr.* **37,** 207–225
36. Khalifat, N., Puff, N., Dliaa, M., and Angelova, M. I. (2012) Amyloid-β and the failure to form mitochondrial cristae: a biomimetic study involving artificial membranes. *J. Alzheimers Dis.* **28,** 33–48
37. Hong, W. K., Han, E. H., Kim, D. G., Ahn, J. Y., Park, J. S., and Han, B. G. (2007) Amyloid-β-peptide reduces the expression level of mitochondrial cytochrome oxidase subunits. *Neurochem. Res.* **32,** 1483–1488

38. Rosen, K. M., Veereshwarayya, V., Moussa, C. E., Fu, Q., Goldberg, M. S., Schlossmacher, M. G., Shen, J., and Querfurth, H. W. (2006) Parkin protects against mitochondrial toxins and β-amyloid accumulation in skeletal muscle cells. *J. Biol. Chem.* **281,** 12809–12816
39. Askanas, V., Engel, W. K., and Nogalska, A. (2009) Inclusion body myositis. A degenerative muscle disease associated with intra-muscle fiber multi-protein aggregates, proteasome inhibition, endoplasmic reticulum stress and decreased lysosomal degradation. *Brain Pathol.* **19,** 493–506
40. Nogalska, A., D'Agostino, C., Terracciano, C., Engel, W. K., and Askanas, V. (2010) Impaired autophagy in sporadic inclusion-body myositis and in endoplasmic reticulum stress-provoked cultured human muscle fibers. *Am. J. Pathol.* **177,** 1377–1387
41. Boncompagni, S., Rossi, A. E., Micaroni, M., Hamilton, S. L., Dirksen, R. T., Franzini-Armstrong, C., and Protasi, F. (2009) Characterization and temporal development of cores in a mouse model of malignant hyperthermia. *Proc. Natl. Acad. Sci. U.S.A.* **106,** 21996–22001
42. Zissimopoulos, S., Docrat, N., and Lai, F. A. (2007) Redox sensitivity of the ryanodine receptor interaction with FK506-binding protein. *J. Biol. Chem.* **282,** 6976–6983
43. Zissimopoulos, S., and Lai, F. A. (2006) Redox regulation of the ryanodine receptor/calcium release channel. *Biochem. Soc. Trans.* **34,** 919–921
44. Allen, D. G., Lännergren, J., and Westerblad, H. (1995) Muscle cell function during prolonged activity. Cellular mechanisms of fatigue. *Exp. Physiol.* **80,** 497–527
45. Wolosker, H., Rocha, J. B., Engelender, S., Panizzutti, R., De Miranda, J., and de Meis, L. (1997) Sarco/endoplasmic reticulum Ca^{2+}-ATPase isoforms. Diverse responses to acidosis. *Biochem. J.* **321,** 545–550
46. Webster, N. J., Ramsden, M., Boyle, J. P., Pearson, H. A., and Peers, C. (2006) Amyloid peptides mediate hypoxic increase of L-type Ca^{2+} channels in central neurones. *Neurobiol. Aging* **27,** 439–445
47. Scragg, J. L., Fearon, I. M., Boyle, J. P., Ball, S. G., Varadi, G., and Peers, C. (2005) Alzheimer's amyloid peptides mediate hypoxic up-regulation of L-type Ca^{2+} channels. *FASEB J.* **19,** 150–152
48. Kim, S., and Rhim, H. (2011) Effects of amyloid-β peptides on voltage-gated L-type $Ca_V1.2$ and $Ca_V1.3$ Ca^{2+} channels. *Mol. Cells* **32,** 289–294
49. Lopez, J. R., Lyckman, A., Oddo, S., Laferla, F. M., Querfurth, H. W., and Shtifman, A. (2008) Increased intraneuronal resting Ca^{2+} in adult Alzheimer's disease mice. *J. Neurochem.* **105,** 262–271